

# Liquid-liquid phase transition in an atomistic model glass former

Thomas Speck,<sup>1</sup> C. Patrick Royall,<sup>2,3,4</sup> and Stephen R. Williams<sup>5</sup>

<sup>1</sup>*Institut für Physik, Johannes Gutenberg-Universität Mainz, Staudingerweg 7-9, 55128 Mainz, Germany*

<sup>2</sup>*HH Wills Physics Laboratory, University of Bristol, Bristol BS8 1TL, UK*

<sup>3</sup>*School of Chemistry, University of Bristol, Bristol BS8 1TS, UK*

<sup>4</sup>*Centre for Nanoscience and Quantum Information, Bristol BS8 1FD, UK*

<sup>5</sup>*Research School of Chemistry, Australian National University, Canberra, ACT 0200, Australia*

Whether the glass transition is related to an underlying thermodynamic singularity or whether it is a purely kinetic phenomenon is a major outstanding question in condensed matter physics. The main challenge one faces when studying supercooled liquids and glasses is of course that the dynamics of the constituent particles slows by many orders of magnitude. Thus it is hard to approach any possible transition with computer simulations, and one must extrapolate over many decades in relaxation time assuming no qualitative change in the system's behaviour. This limits the use of simulation, which would otherwise provide the detailed information with which one could discriminate between the numerous competing theoretical approaches. Here we make progress by introducing a sampling method that enables previously inaccessible dynamical regimes to be directly studied in an atomistic model glass former. Our study reveals a peak in the specific heat capacity, which we interpret as a drop in the density of states. Rather than being related to the formation of an “ideal glass”, we provide evidence that the heat capacity peak is related to a liquid-liquid transition to a state rich in locally stable geometric motifs. This second liquid is structurally distinct from that observed at high temperature but remains amorphous.

## Introduction

The concept of a liquid-liquid transition (LLT) between two distinct (metastable) supercooled liquids has attracted considerable interest [1, 2]. Some evidence for LLTs has been obtained in model systems [3, 4] and metallic glass formers [2, 5]. Such transitions remain highly controversial both in metallic systems [6] and molecular systems such as water [7, 8]. The application of thermodynamic concepts is, strictly speaking, not admissible due to the finite lifetime of both liquids, but might be a practical tool in situations where this lifetime vastly exceeds both typical measurement times and structural relaxation times. Typical glass forming liquids often fall into this category.

At the glass transition the liquid falls out of equilibrium, in particular it acquires a memory of its preparation. Although this event precludes a direct observation, many theoretical approaches invoke an underlying thermodynamic transition. Examples include the transition to an amorphous ground state (the “ideal glass”) [9, 10] or a LLT to a state with the atoms arranged in certain geometric motifs or *locally favoured structures* [1, 11]. The pinning (or confinement) of particles has been argued to shift a thermodynamic transition into the accessible regime [12, 13], and a loss of configurational entropy indicated by a peak in the heat capacity [14] has been reported.

Although convincing evidence for an underlying thermodynamic transition remains elusive, it has been demonstrated recently that there is a *dynamical* transition in the space of *trajectories*, *i.e.*, sequences of configurations. Under biased sampling trajectories of sufficient length undergo a first-order transition between an *active* phase (the supercooled liquid) and a dynamically

*inactive* phase, which has been observed both in idealized lattice models [15] and in simulations of atomistic model glass formers [16, 17]. The latter case affords a systematic computational means of preparing exceptionally stable glass states [17, 18] (see also Ref. [19] for other methods to prepare ultra-stable glasses). One suitable means to generate such transitions in trajectory space is to employ biased sampling of trajectories based on an order parameter characterizing *time-averaged* populations of locally favoured structures (LFS) [17]. Connections between these inactive phases prepared *in silico* and those found in experiment (where there is no bias) are only just beginning to be addressed [20].

Configurations visited in the inactive phase have interesting properties. While still amorphous, they are very stable with very large structural relaxation times. Moreover, steepest descent quenches to *inherent states* indicate that the inactive phase probes configurations very deep in the energy landscape relative to “normal” liquid configurations [17, 18]. The latter observation opens the possibility that these configurations have a finite weight also in the equilibrium Boltzmann ensemble at a lower temperature. A major obstacle in probing the link between deeply supercooled liquids and the inactive phase is that in glass formers time scales are far beyond direct computational methods such as molecular dynamics (MD) simulations. Here, to circumvent this problem we employ a reweighting technique to gain insights into the behavior at very low temperatures from data sampled at a mildly supercooled temperature. The technique exploits the time-scale separation between vibrations and structural relaxation [21], whereby the relaxation time is nevertheless small enough to allow efficient sampling. We find a peak in the specific heat capacity  $c_v$  at a temperature  $T_* > T_K$  higher than the extrapolated Kauzmann

temperature  $T_K$  corresponding to an “ideal glass” state. Moreover, we show that this peak is related to the transition in trajectory space to the dynamical phase rich in LFS [17]. From this numerical evidence we conclude the existence of a LLT at  $T_*$  from the supercooled liquid to a state rich in LFS.

### Model

We consider the Kob-Andersen binary mixture [22], a well studied atomistic glass former that consists of 80% large particles (A) and 20% small particles (B) interacting through truncated and shifted Lennard-Jones pair potentials. We employ the original potential parameters. All numerical values are reported in Lennard-Jones units with respect to the large particles, and we set Boltzmann’s constant to unity. We study a system of  $N = 216$  particles at number density  $N/V = 1.2$  in a box with constant volume  $V$ .

Our numerical scheme [17] harvests trajectories with fixed number of configurations  $K$  at temperature  $T_s = 0.6$  through a combination of transition path sampling moves (shifting and half-shooting moves) to generate trial trajectories [23], the Metropolis criterion to accept or reject trajectories, and replica exchange between quadratic biasing potentials of the appropriate order parameter: the inherent state energy per particle  $\phi$  and the population  $\mathcal{N}$  of particles in LFS, which couples to an external field  $\mu$ . In this model, the LFS is a biccapped square antiprism [24, 25].

In particular, we calculate the average of an observable  $A$  at different state points with

$$\langle A \rangle(T, \mu) \equiv \frac{\langle A e^{-(1/T - 1/T_s)N\phi + \mu\mathcal{N}} \rangle_0}{\langle e^{-(1/T - 1/T_s)N\phi + \mu\mathcal{N}} \rangle_0}. \quad (1)$$

The brackets  $\langle \cdot \rangle_0$  denote the average over the sampled trajectories using their unbiased equilibrium weight as indicated by the subscript. This expression is evaluated employing the multistate Bennett acceptance ratio method [26]. Assuming that inherent state energies and vibrational free energy decouple (as appropriate here), it is straightforward to show that averages of observables  $A = A(\phi)$  that only depend on  $\phi$  are equilibrium averages in the absence of the field ( $\mu = 0$ ). Thus by reweighting according to the inherent state energy, we access configurations corresponding to temperatures beyond the range of normal simulations. See Methods for further details.

**Energy landscape.** We first study the statistics of inherent states [27]. Let  $\Omega(\phi) \propto \Omega_\infty e^{N\sigma(\phi)} \delta\phi$  be the number of *amorphous* inherent states with energy per particle  $\phi$  within an interval  $\phi \pm \delta\phi/2$ , where  $\sigma(\phi)$  is the enumeration function. This scenario is sketched in Fig. 1(a). Here,  $\Omega_\infty \simeq e^{N s_\infty}$  is the maximal available volume in configuration space. In the limit of large  $N$ , the number  $\Omega$  is either extensive or becomes exponentially small. Hence, in the thermodynamic limit, the extensive

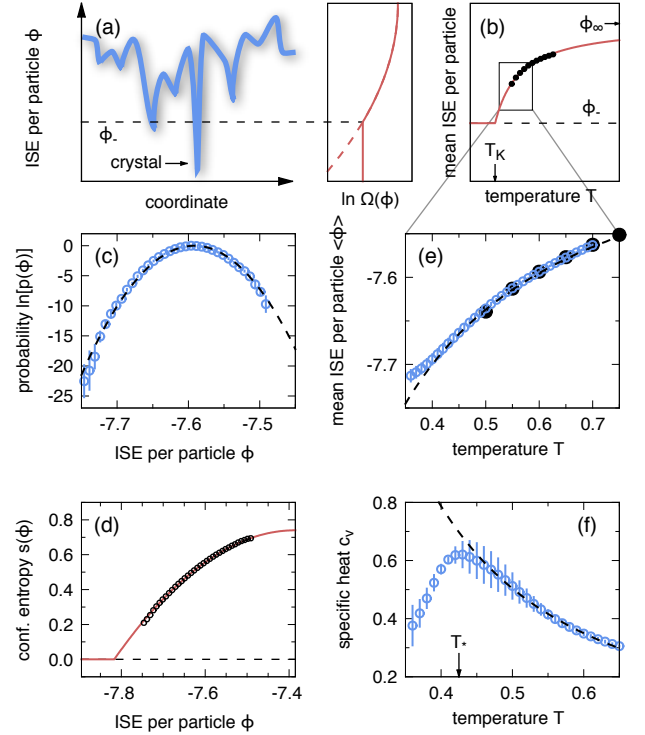


FIG. 1: Statistical description of inherent states: (a) Caricature of inherent state energies (ISE)  $\phi$  along an arbitrary coordinate. Number of amorphous inherent states within a given energy interval is  $\Omega(\phi)$ . Exponentially small  $\Omega(\phi)$  below  $\phi_-$  (dashed continuation) corresponding to vanishing configurational entropy in the thermodynamic limit (solid line). (b) Mean energy  $\langle \phi \rangle$ , which becomes equal to constant  $\phi_-$  below  $T_K$ . Symbols show inherent state energies from conventional MD simulations. (c) Logarithm of the sampled probability distribution  $p(\phi)$  for the sampling temperature  $T_s = 0.6$ . Dashed line is a Gaussian fit. (d) Configurational entropy  $s(\phi)$ . The line is the expected quadratic behavior, the symbols are the data from (c) without temperature-bias. (e) Mean energy  $\langle \phi \rangle$  as a function of temperature  $T$  corresponding to the indicated range in (b). Shown are results from conventional MD simulations ( $\bullet$ ) and results employing our reweighting scheme ( $\circ$ ). Dashed line is the prediction Eq. (2). (f) Heat capacity  $c_v$  calculated from the inherent energy fluctuations exhibits a peak around  $T_* \simeq 0.425$ . Dashed line is heat capacity for quadratic enumeration function.

configurational entropy becomes  $\ln \Omega(\phi) \simeq N s(\phi)$  with  $s(\phi) = s_\infty + \sigma(\phi)$  for  $\phi \geq \phi_-$  and  $s = 0$  for extreme energies  $\phi < \phi_-$ . We assign a temperature to the inherent structures based on  $d\sigma/d\phi = 1/T$ . First pointed out by Kauzmann in 1948 [28], the possibility that  $\phi_-$  is reached at a finite temperature  $T_K$  has intrigued scientists ever since. Figuratively speaking, at this temperature the system would “run out” of amorphous configurations and would undergo a thermodynamic phase transition to an ideal glass with constant inherent state energy  $\phi_-$ , see Fig. 1(b).

In our simulations, we access the distribution  $p(\phi)$

of inherent state energies, which for  $T_s$  is plotted in Fig. 1(c). In agreement with previous studies [21, 29], we find that this distribution is well described by a Gaussian. Moreover, it has been demonstrated that at low enough temperature (including the sampling temperature  $T_s = 0.6$  used here) the vibrational free energy is independent of  $\phi$  to a very good approximation [21]. We can thus extract the quadratic enumeration function  $\sigma(\phi) = -(\phi - \phi_\infty)^2/J^2$  from the measured distribution with fitted maximal energy  $\phi_\infty \simeq -7.385$  and scale  $J \simeq 0.502$ . The resulting configurational entropy is plotted in Fig. 1(d) using the value  $s_\infty \simeq 0.74$  reported previously [21]. It demonstrates that our numerical scheme is able to cover a wide range of inherent states and that the configurational entropy is indeed very well described by a quadratic function. For the thermal average one finds

$$\langle \phi \rangle = \phi_\infty - \frac{J^2}{2T} \quad (\phi \geq \phi_-). \quad (2)$$

Extrapolating the quadratic form for  $\sigma(\phi)$  to lower energies, one easily derives  $T_K = J/(2\sqrt{s_\infty})$  for the Kauzmann temperature yielding  $T_K \simeq 0.29$  for the present system [21]. Whether such an extrapolation is meaningful is debated, *e.g.*, Stillinger has pointed out that the “melting” of an ideal glass through defects would imply  $T_K = 0$  [30].

In Fig. 1(e) the mean inherent state energy  $\langle \phi \rangle$  is shown as a function of temperature. Down to  $T = 0.5$  we have run conventional MD simulations and determined the average  $\langle \phi \rangle$ , which agrees well with Eq. (2). Also plotted are the average inherent state energies obtained through reweighting our simulation results obtained at  $T_s = 0.6$  to different temperatures, which agree with both the MD simulations and the prediction Eq. (2). Strikingly, at lower temperatures we observe a deviation from the behavior expected for a quadratic enumeration function. This becomes even more pronounced when we consider the susceptibility, *i.e.*, the specific heat capacity

$$c_v = \frac{\partial \langle \phi \rangle}{\partial T} = \frac{\langle \phi^2 \rangle - \langle \phi \rangle^2}{T^2} \quad (3)$$

of the inherent states. From Eq. (2) we expect  $c_v = \frac{1}{2}(J/T)^2$  for  $T > T_K$  and  $c_v = 0$  below the Kauzmann temperature  $T_K$ . As shown in Fig. 1(f), the heat capacity drops below the expected behavior already for a temperature  $T_* \simeq 0.425$  somewhat larger than the Kauzmann temperature.

### Transitions in trajectory space

In order to elucidate the physical origin of this drop in  $c_v$ , we now turn to the active-inactive transition [17] and make the conceptual leap from configurations to trajectories. We spawn trajectories (symbolically denoted  $x(t)$ , where  $t$  is time) of length  $t_{\text{obs}} = K\Delta t$  by integrating backward and forward in time. To characterize trajectories, we count the number  $\mathcal{N}[x(t)]$  of particles that

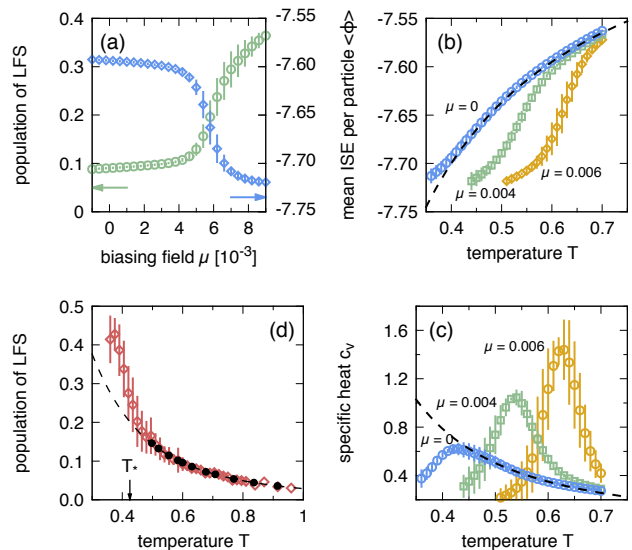


FIG. 2: Transition in trajectory space: (a) Mean population  $n$  (left axis) and the mean inherent state energy  $\langle \phi \rangle$  (right axis) as a function of  $\mu$ . Both observables show an abrupt change around  $\mu_* \simeq 5.8 \times 10^{-3}$ . (b) The mean energy  $\langle \phi \rangle$  as a function of temperature extended to  $\mu > 0$ , cf. Fig. 1(d). (c) Specific heat for the same values of  $\mu$ , cf. Fig. 1(f). (d) Population ( $\bullet$ ) of LFS from conventional MD simulations. The dashed line is an extrapolation of this data using the phenomenological function  $n = (1 + (T/0.25)^{2.5})^{-1}$ . In comparison, results ( $\diamond$ ) from “thermalized” MD simulations show a jump, see text for further details.

reside in LFS. In analogy to conventional thermodynamics, we couple the order parameter  $\mathcal{N}$  to an external field  $\mu$  akin to a chemical potential difference. We consider the perturbed distribution of trajectories [16]

$$P_\mu[x(t)] \propto P_0[x(t)]e^{\mu\mathcal{N}[x(t)]}, \quad (4)$$

which favors a large population of the structural motif for  $\mu > 0$ . Although we sample trajectories, for our analysis we only consider the initial and central configurations, which we characterize in terms of the inherent state energy  $\phi$  as before and, in addition, the population  $n = \langle N_{\text{LFS}} \rangle / N$ , where  $N_{\text{LFS}}$  is the number of particles in LFS in the central configuration. In Fig. 2(a), both these quantities are plotted as a function of the field  $\mu$  at the sampling temperature  $T_s = 0.6$ . Around  $\mu_* \simeq 5.6 \times 10^{-3}$ , we observe a sudden change from the liquid containing few LFS ( $n \simeq 0.09$ ) to a phase rich in LFS. At the same time, the average inherent state energy drops from  $\simeq -7.61$  to below  $-7.7$ , which corresponds to a (unbiased) configurational temperature of less than 0.4, cf. Figs. 1(e) and 2(b). The steepness of the transition and the value of  $\mu_*$  depend strongly on the trajectory length  $K$  and are compatible with a first-order transition [17].

In order to relate the statistics of the potential energy landscape with the dynamical transition, we extend our

analysis by considering the trajectory weight

$$P_{\mu,T} \propto P_0 \exp \{ \mu \mathcal{N} - (1/T - 1/T_s) \mathcal{N} \phi \}. \quad (5)$$

This “continuation” allows us to study the system as a function of both variables  $\mu$  and  $T$ . In Fig. 2(b) we show the average inherent state energy  $\langle \phi \rangle$  as a function of  $T$  for three different values of  $\mu$ . We observe a clear drop of the inherent state energy, which is shifted to lower temperatures as  $\mu$  is lowered. As expected from this behavior, the heat capacity Eq. (3) shown in Fig. 2(c) exhibits a peak that is also shifted to lower temperatures. As the temperature is reduced, the peak height drops. This drop is consistent with a dynamical critical point at  $(T_c > T_*, \mu > 0)$  at which the susceptibility may diverge [31], see also Fig. 3(b).

### Linking the dynamical transition and $c_v$ peak

Extrapolating the dynamical transition to  $\mu = 0$  suggests that the zero-bias  $c_v$  peak would also correspond to a transition to a (static) LFS-rich state. However, studying this proposed thermodynamic LLT with MD simulations is not straightforward due to the huge computational effort to properly equilibrate the system at the required temperatures. Moreover, the scenario of a first order transition implies that the liquid becomes metastable with respect to the LFS-rich state (and possibly also to crystallisation). As a consequence, the relevant configurations might not be found by straightforward molecular dynamics. Still, these configurations contribute to equilibrium averages at low temperatures due to their low energies, see Fig. 2(d). Here we have “thermalized” configurations harvested from the biased simulations with conventional molecular dynamics at the configurational temperature  $T$  of the inherent state [inverting Eq. (2)] for  $t = 150$ , which is sufficient for the system to undergo  $\beta$ -relaxation. Indeed, we see a sharper rise in the LFS population upon cooling compared to the extrapolated behaviour. Noting that since the LFS population is bounded to be  $n < 1$  it appears that indeed there is a transition around  $T_* \simeq 0.425$  to an LFS-rich state.

In Fig. 3(a) we present the phase diagram between the supercooled liquid and the LFS-rich phase as signaled by the maximum of the specific heat. Also shown are distributions of the inherent state energies at configurational temperature  $T = 0.55$  for three values of  $\mu$ . Close to coexistence one discerns two populations having different inherent state energies that reverse their relative weights passing through the phase boundary. This observation is again compatible with the scenario of a phase transition. Note that for  $\mu \neq 0$  the position of the phase boundary and also the peak value of the heat capacity depends on the value of  $K$  used to sample trajectories. However, for two trajectory lengths  $K = 100$  and  $K = 60$  we have checked that for  $\mu = 0$  both  $T_*$  and the value of  $c_v$  agree as expected. Finally, in Fig. 3(b) a sketch of the

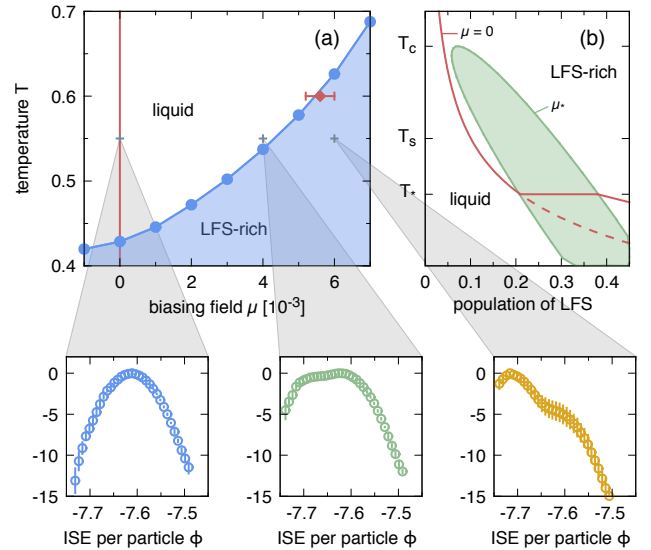


FIG. 3: Phase diagram: (a) The symbols (•) show where the specific heat capacity  $c_v$  reaches its maximum as a function of both  $T$  and  $\mu$  for  $K = 100$  (the line is a guide to the eye). The single diamond indicates the position of the dynamic phase transition and its statistical uncertainty. Shown below for  $T = 0.55$  are probability distributions  $\ln[p(\phi)]$  of the inherent state energy per particle for the three indicated values of the biasing field (dynamical chemical potential)  $\mu$ . One distinguishes two populations at different inherent state energies, which we ascribe to the liquid and LFS-rich phases, respectively. (b) Sketch of the corresponding  $n$ - $T$  plane: Below the critical temperature  $T_c$  phase coexistence is possible (shaded area bounded by  $\mu_*$ ). The solid red line corresponds to  $\mu = 0$ , where the dashed line indicates the metastable branch below  $T_*$ . At  $T_*$  one has  $\mu_* = 0$  and a thermodynamic LLT occurs.

corresponding  $n$ - $T$  plane is shown. Below a critical temperature, dynamical coexistence of liquid and LFS-rich phase is possible. Unconstrained equilibrium dynamics corresponds to a vanishing field  $\mu = 0$ , which lies in the liquid region as long as  $\mu_* > 0$ . The observed jump in the population suggests that at  $T_*$  a LLT occurs, whereby  $\mu_* = 0$ .

### Conclusions

We have developed a reweighting technique that allows us to access a wide range of inherent states and thus exceptionally low temperatures in a model glass forming liquid. This opens a perspective of what actually happens as the system starts to run out of configurational entropy. We find a peak in the specific heat, which occurs at a temperature  $T_* \simeq 0.425$  above the Kauzmann temperature  $T_K \simeq 0.29$  (estimated under the condition that the quadratic behavior of the enumeration function continues to lower energies [21]). This transition is distinct from the dynamical crossover to an energy landscape dominated regime since we sample configurations

and determine their weight solely based on their energy. In other words, our reweighting is not affected by sampling limitations that usually prevent simulation techniques from sampling lower temperatures.

The connection with a dynamical phase transition at a higher temperature to a state rich in locally favoured structures enables insights into the nature of the transition underlying the  $c_v$  peak. The dynamical transition, which occurs under a non-zero field controlling the chemical potential difference between liquid and LFS particles, also features a  $c_v$  peak, and upon reducing the chemical potential we find a line of maxima connecting both transitions. We thus interpret this line as the phase boundary corresponding to a liquid-liquid transition between a low-temperature LFS-rich phase and the normal supercooled liquid. Such a transition is in accord with the geometric frustration approach [11].

While an LLT will have significant consequences for the glass forming properties of the studied model, we have not attempted to identify a glass transition line, which will depend strongly on time scales. An important question lies in the generality of our findings. We have considered perhaps the most popular atomistic glassformer. Our findings should certainly be checked with other models. The Kob-Andersen model we have considered is based on a metallic glass, NiP. Indeed a number of metallic glassformers are known to undergo LLTs [2, 5]. Regarding the glassforming properties we note links between LLTs and fragile-to-strong transitions in both metallic [32] and molecular [33] glassformers. If such a connection between LLTs and strong low-temperature liquids can be established, the consequences for a thermodynamic glass transition are profound as in the limit of a perfectly strong liquid there is no transition.

## Methods

Trajectories are stored as sequences  $X = (x_{-K/2}, \dots, x_{K/2})$  of  $K + 1$  configurations  $x_i$ . We

use a stochastic thermostat to control temperature, *i.e.*, we draw all particle velocities from a Maxwell-Boltzmann distribution before integrating for a time  $\Delta t = 1.5$  using the velocity Verlet algorithm and storing the next configuration. In addition, inherent states  $\hat{x}_i$  are obtained by a minimization of the potential energy  $\Phi(x)$  of configurations using the FIRE algorithm [34]. To make the harvesting of millions of trajectories feasible, we limit the number of FIRE iterations to 1,000. Hence, the reported values for  $\phi = \Phi/N$  should be understood as upper (although tight) bounds to the true inherent state energies.

We perform two independent sets of biased simulations using quadratic bias functions of the relevant observable that are spaced equidistantly. First, we employ the total number  $\mathcal{N}[X] \equiv \sum_{i=-K/2}^{K/2} \sum_{k=1}^N h_k(x_i)$  of particles participating in LFS motifs in the whole trajectory, where  $h_k(x)$  is an indicator function that is unity if particle  $k$  of configuration  $x$  is part of an LFS and zero otherwise [17]. Second, we bias trajectories using the inherent state energy  $\phi$ . For each umbrella we harvest 120,000 trajectories in the first run and 60,000 trajectories in the second run and combine the data. To estimate errors, the data is split into three sets and analyzed independently.

**Acknowledgments.** CPR acknowledges the Royal Society and European Research Council (ERC consolidator grant NANOPRS, project number 617266). This work was carried out using the computational facilities of the Advanced Computing Research Centre, University of Bristol. We thank L. Berthier, D. Chandler, P. Harrowell, J. Garrahan, R. Jack and H. Tanaka for discussions and helpful comments.

- 
- [1] H. Tanaka, J. Phys.: Cond. Matter **11**, L159 (1999).
  - [2] P. F. McMillan, M. Wilson, M. C. Wilding, D. Daisenberger, M. Mezouar, and G. N. Greaves, J. Phys.: Cond. Matter **19**, 415101 (2007).
  - [3] M. Elenius, T. Oettel, and M. Dzugutov, J. Chem. Phys. **133**, 174502 (2010).
  - [4] P. Ronceray and P. Harrowell, Phys. Rev. Lett. **112**, 017801 (2014).
  - [5] S. Wei, F. Yang, J. Bednarcik, I. Kaban, O. Shuleshova, A. Meyer, and R. Busch, Nat. Comm. **4**, 2083 (2013).
  - [6] A. C. Barnes, L. B. Skinner, P. S. Salmon, A. Bytchkov, I. Pozdnyakova, T. O. Farmer, and H. E. Fischer, Phys. Rev. Lett. **103**, 225702 (2009).
  - [7] D. T. Limmer and D. Chandler, J. Chem. Phys. **135**, 134503 (2011).
  - [8] J. C. Palmer, F. Martelli, Y. Liu, R. Car, A. Z. Panagiotopoulos, and P. G. Debenedetti, Nature **510**, 385 (2014).
  - [9] A. Cavagna, Phys. Rep. **476**, 51 (2009).
  - [10] L. Berthier and G. Biroli, Rev. Mod. Phys. **83**, 587 (2011).
  - [11] G. Tarjus, S. A. Kivelson, Z. Nussinov, and P. Viot, J. Phys.: Condens. Matter **17**, R1143 (2005).
  - [12] C. Cammarota, A. Cavagna, I. Giardinà, G. Gradenigo, T. S. Grigera, G. Parisi, and P. Verrocchio, Phys. Rev. Lett. **105**, 055703 (2010).
  - [13] L. Berthier, Phys. Rev. E **88**, 022313 (2013).
  - [14] D. A. Martín, A. Cavagna, and T. S. Grigera, ArXiv p. 1407.6322 (2014).
  - [15] M. Merolle, J. P. Garrahan, and D. Chandler, Proc. Natl. Acad. Sci. U.S.A. **102**, 10837 (2005).
  - [16] L. O. Hedges, R. L. Jack, J. P. Garrahan, and D. Chan-

- dler, *Science* **323**, 1309 (2009).
- [17] T. Speck, A. Malins, and C. P. Royall, *Phys. Rev. Lett.* **109**, 195703 (2012).
  - [18] R. L. Jack, L. O. Hedges, J. P. Garrahan, and D. Chandler, *Phys. Rev. Lett.* **107**, 275702 (2011).
  - [19] S. Singh, M. D. Ediger, and J. J. de Pablo, *Nature Materials* **12**, 139? (2013).
  - [20] A. S. Keys, D. Chandler, and J. P. Garrahan, *arXiv:1401.7206* (2014).
  - [21] F. Sciortino, W. Kob, and P. Tartaglia, *Phys. Rev. Lett.* **83**, 3214 (1999).
  - [22] W. Kob and H. C. Andersen, *Phys. Rev. Lett.* **73**, 1376 (1994).
  - [23] C. Dellago, P. G. Bolhuis, and P. L. Geissler, *Adv. Chem. Phys.* **123**, 1 (2002).
  - [24] D. Coslovich and G. Pastore, *J. Chem. Phys.* **127**, 124504 (2007).
  - [25] A. Malins, J. Eggers, H. Tanaka, and C. P. Royall, *Fara-day Discuss.* **167**, 405 (2013).
  - [26] M. R. Shirts and J. D. Chodera, *J. Chem. Phys.* **129**, 124105 (2008).
  - [27] P. G. Debenedetti and F. H. Stillinger, *Nature* **410**, 259 (2001).
  - [28] W. Kauzmann, *Chem. Rev.* **43**, 219 (1948).
  - [29] S. Büchner and A. Heuer, *Phys. Rev. E* **60**, 6507 (1999).
  - [30] F. H. Stillinger, *J. Chem. Phys.* **88**, 7818 (1988).
  - [31] Y. S. Elmatad, R. L. Jack, D. Chandler, and J. P. Garrahan, *Proc. Nat. Acad. Sci.* **107**, 12793 (2010).
  - [32] C. Zhang, L. Hu, Y. Yue, and J. C. Mauro, *J. Chem. Phys.* **133**, 014508 (2010).
  - [33] F. Mallamace, C. Branca, C. Corsaro, N. Leone, J. Spooren, S.-H. Chen, and H. E. Stanley, *Proc. Natl. Acad. Sci. U.S.A.* **107**, 22457?22462 (2010).
  - [34] E. Bitzek, P. Koskinen, F. Gähler, M. Moseler, and P. Gumbsch, *Phys. Rev. Lett.* **97**, 170201 (2006).